

Sub-20 kHz low frequency noise near ultraviolet miniature external cavity laser diode

RONAN KERVAZO,¹ ANTOINE CONGAR,² GEORGES PERIN,¹ LAURENT LABLONDE,³ RAPHAËL BUTTÉ,⁴ NICOLAS GRANDJEAN,⁴ LOÏC BODIOU,¹ JOËL CHARRIER,¹ AND STÉPHANE TREBAOL^{1,*}

¹Univ Rennes, CNRS, Institut FOTON – UMR 6082, F-22305 Lannion, France

²Oxxius, 4 rue Louis de Broglie, 22300 Lannion, France

³Exail, rue Paul Sabatier, Lannion, France

⁴Institute of Physics, École Polytechnique Fédérale de Lausanne (EPFL), CH-1015 Lausanne, Switzerland

*stephane.trebaol@univ-rennes.fr

Abstract: We present a compact InGaN fiber Bragg grating (FBG) semiconductor laser diode operating below 400 nm in the single-mode emission regime. This compact coherent laser source exhibits an intrinsic linewidth of 14 kHz in the near-UV range. We report a side-mode suppression ratio reaching up to 40 dB accompanied by a mW-level output power. Furthermore, the properties of the FBG, including its central wavelength, bandwidth, and reflectivity, can be readily customized to fulfill specific requirements. The combination of small footprint design, wavelength tunability, low frequency noise, and access to the fibered output signal positions these FBG laser systems as strong candidates for hybridization into integrated photonic platforms tailored for quantum information processing and metrology.

1. Introduction

Nowadays, laser diodes are essential elements for the development of compact photonic devices. They offer the opportunity of combining good performances in terms of linewidth, optical power and frequency noise [1–3]. The needs in the field of optical telecommunications have enabled the development of compact laser diodes mainly in the telecom C-band. The implementation of compact laser diodes with low-frequency noise at visible wavelengths covering the near-ultraviolet to infrared spectral range is a technological challenge recently addressed by several research groups [4–9]. The objective is to provide laser diodes capable of meeting several application requirements in the fields of classical and quantum sensors and the metrology of optical frequencies for the production of compact optical clocks [10–12]. Indeed, such clocks require the use of narrow-spectrum and low-frequency noise lasers at visible wavelengths for cooling, capturing and manipulating atoms or ions [11,13–15]. Commercial laser devices offering the necessary performances are usually based on the use of an external cavity involving a diffraction grating that does not provide the desired compactness and mechanical robustness for applications outside laboratories. However, recent demonstrations based on compact external cavities, such as high-quality factor gallery mode [2,7] resonators or integrated optical resonators [4,5], offer interesting perspectives. The reported performances approach the expressed needs, namely linewidths on the order of the MHz and optical powers in the mW range. Nevertheless, the performance of state-of-the-art optical clocks is still limited by the frequency noise floor of the lasers used [16]. Indeed, efforts are needed to lower this noise floor by increasing the finesse of the external cavity, which can be obtained by reducing the propagation losses and by increasing the reflectivity of the output mirror. Fiber Bragg gratings [17] (FBGs) are suitable devices for deporting the external cavity in the collection fiber, combining low propagation losses and a wavelength-selective mirror whose reflectivity and bandwidth can be widely adjusted to find the right optical power/finesse trade-off. Moreover, the Bragg center wavelength can be finely adjusted by less than 0.1 nm with current

fabrication methods [18]. In addition, fiber gratings exhibit a significantly lower sensitivity to temperature fluctuations compared to laser diode waveguides [19]. This characteristic provides the opportunity to operate without thermal regulation. Initially implemented in the C-band for wavelength-division multiplexing applications [20,21], research works on fiber Bragg grating lasers (FGLs) are now reported at various optical wavelengths [8,22]. Indeed, due to their exceptional wavelength accuracy and stability, fiber gratings can serve as frequency references, enabling single-mode laser frequency emissions that precisely align with the requirements of atomic spectroscopy and metrology [10,23].

In this paper, we study a small-footprint configuration of a UV laser diode emitting at 399.6 nm subject to optical feedback from an FBG. Looking for a trade-off between footprint reduction, ease of integration from one side, and optical stability, output power optimization from the other side brought us to develop a butt-coupled configuration of the FGL. The resulting 2 cm external fibered cavity acts as a spectral filter that strongly improves the spectral performance of the initially multimode laser (Fig. 1). The resulting single-mode laser displays an intrinsic linewidth down to 14 kHz with a mW-fibered-output power. Thanks to the narrowband FBG, a 40 dB side-mode suppression ratio (SMSR) is obtained.

The structure of the laser diode, the fabrication and characterization steps of the Bragg grating contributing to the external cavity are first described. Then, the spectral performances of the laser, in particular the spectrum and frequency noise measurements, are presented.

2. Experimental setup

The architecture of the single-mode laser diode is detailed on Fig. 1.

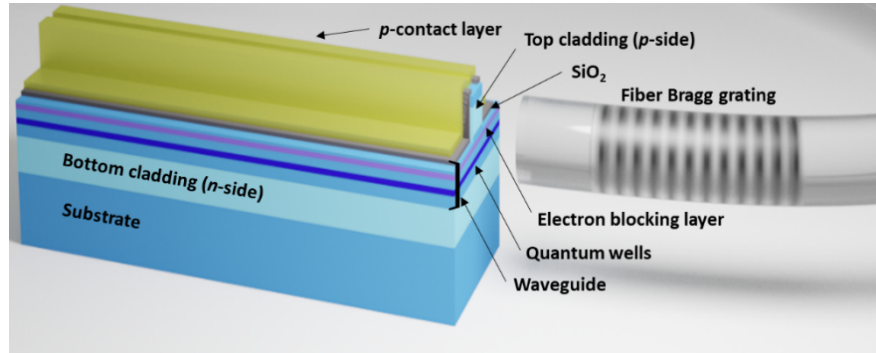


Fig. 1. Schematic of the FBG InGaN laser diode. Details are given in the Supplementary Material (Sec.1)

The laser diode stacking was epitaxially grown using the metalorganic vapor phase epitaxy method on a low threading dislocation density ($\sim 10^6 \text{ cm}^{-2}$) *c*-plane free-standing GaN substrate following the same procedure as described in ref. [24]. The optical gain, centered at 400 nm, is provided by two 4.5-nm-wide InGaN quantum wells separated by 12-nm-undoped $\text{In}_{0.05}\text{Ga}_{0.95}\text{N}$ barriers, while a *p*-AlGaIn electron-blocking layer is present on the *p*-type side of the junction to avoid any electron overflow. The bottom and top claddings are 1 μm and 500 nm thick, respectively. The laser consists of an 800- μm -long ridge structure, which corresponds to a measured Fabry-Perot cavity free spectral range (FSR) of 26 pm. The ridge width is limited to 2.5 μm to ensure single-mode transverse operation. A five-layer dielectric distributed Bragg reflector ($\text{SiO}_2/\text{Ta}_2\text{O}_5$) with a reflectivity of $\sim 95\%$ was deposited on the back mirror facet to maximize the emission directivity. On the opposite output facet, a single SiO_2 layer drops the reflection down to $\sim 9\%$ to improve the sensitivity to optical feedback from the FBG and consequently ease the single-mode operation of the laser. The laser diode temperature fluctuations are reduced to less than 0.01 $^\circ\text{C}$ using a Peltier controller. This temperature control

allows the gain curve to be spectrally tuned by 0.07 nm/K on par with the gain frequency drift values reported in the literature for GaN laser diodes [25].

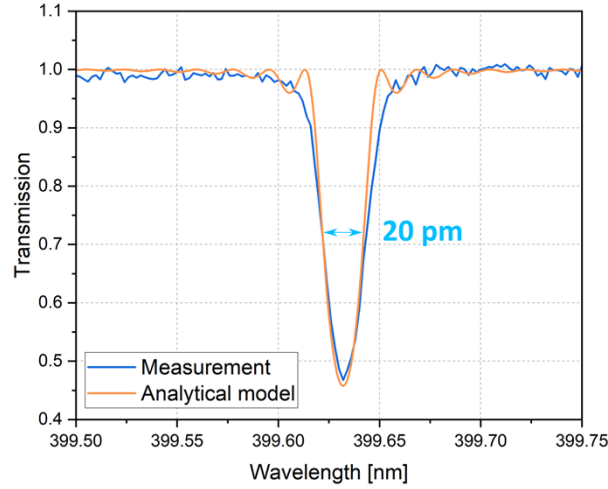


Fig. 2. Fiber Bragg grating transmission measurement (blue curve) and the corresponding simulated spectrum (orange curve). Simulation parameters are the following ones: FBG length = 3 mm, index modulation $\Delta n = 0.40 \times 10^{-4}$. More details are given in the Supplementary Material (Sec.2)

An FBG is associated with the laser diode to form an external cavity. Thus, to obtain a stable single-mode operation and a spectral narrowing of the laser diode under optical feedback, only one longitudinal mode of the laser diode has to be selected by a full-width-at-half maximum (FWHM) of the Bragg grating reflectivity narrower than the FSR of the multimode laser diode to ensure the selection of only one longitudinal mode of the laser diode. The FBG has been designed in consequence.

This mirror is fabricated by exploiting the photosensitivity of a short-wavelength commercially available germanosilicate single-mode fiber. The fiber is transversally exposed to a fringe pattern at a wavelength $\lambda_{uv} = 213$ nm using a 150 mW high-repetition rate nanosecond quintupled Nd:YVO₄ laser [26]. To address the issues for high-quality FBG over Bragg wavelengths ranging from 375 to 410 nm and to achieve Bragg wavelength flexibility, a scanning Talbot interferometer was used [27]. Usually, a direct phase mask writing technique is used to generate these fringes, but there is no accessible commercial solution yet to achieve a 400-nm Bragg wavelength. In a near future, femtosecond laser-written FBGs at short wavelengths could be investigated [28,29].

The transmission spectrum of the 3 mm FBG (Fig. 2, blue curve) displays a reflectivity of 53.5 % and an FWHM evaluated to 20 pm, close to the optical spectrum analyzer (OSA) resolution (10 pm). An analytical model based on the coupled mode theory [17] is used to confirm the adequacy of the design with the measured transmission, as shown in Fig. 2 (orange curve). Further details on the simulation procedure are provided in the Supplementary Material.

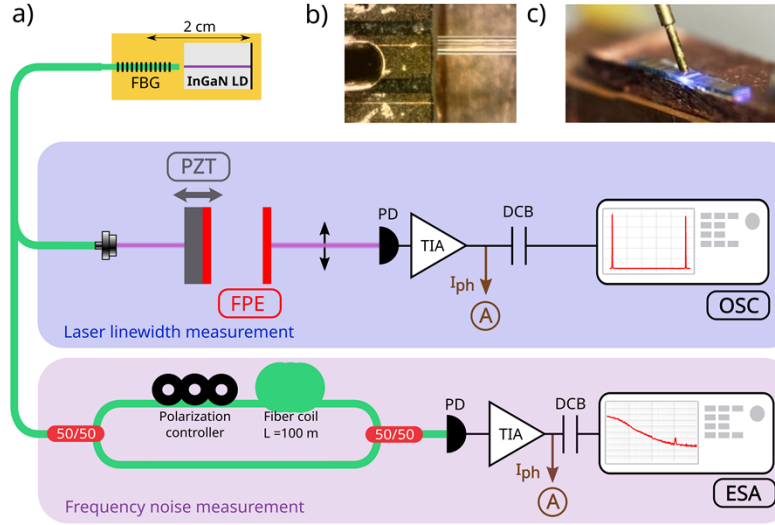


Fig. 3. UV FGL and characterization benches. a) Laser diode structure and experimental setup for linewidth and frequency noise measurements. For linewidth measurements a Fabry-Perot etalon (FPE) is used. One of the mirrors is linearly translated, thanks to a piezo actuator (PZT), to scan the laser line. Frequency noise measurements are performed using a correlated delayed self-homodyne measurement setup composed of an imbalanced fiber-based Mach-Zehnder interferometer that plays the role of frequency noise discriminator. The electrical signals generated by photodiodes (PD) are directed to both an oscilloscope (OSC) and an electrical spectrum analyzer (ESA) via transimpedance amplifiers (TIA) and DC-blocks (DCB). For the measurement of DC photocurrents, a multimeter (A) is used. b) Top view of the InGaN Fabry-Perot laser diode butt-coupled to the FBG. c) Picture of the UV Fabry-Perot laser under electrical pumping.

The external FBG reflector is butt-coupled to the laser diode as shown in Fig. 3a). The external cavity is approximately 2 cm long and the residual gap between the cleaved fiber and the laser diode mirror output is evaluated to be less than 10 μm . The optical feedback at the Bragg wavelength of the narrowband FBG aims to select the nearest longitudinal mode of the Fabry-Perot type semiconductor laser. This can be obtained since the FBG linewidth (20 pm) is narrower than the laser diode FSR (26 pm). Such butt-coupled approach avoids the use of bulky lenses as in extended external cavity approaches hence improving the robustness to mechanical vibrations and thus the spectral performances.

3. Results and discussion

3.1 Optical spectrum narrowing

The optical spectrum of the laser diode was first characterized without Bragg grating (gray curve in Fig. 4a). Without feedback, the optical spectrum of the diode reveals a multimode operation with a maximum SMSR on the order of 20 dB. By carefully aligning the FBG in front of the Fabry-Perot laser diode output, the optical spectrum collapses in a stable single-mode operation. Thus, in its FGL configuration, the laser spectrum bandwidth is drastically reduced and exhibits a single-mode lasing operation at the Bragg wavelength with a 40 dB SMSR for a pump current of 124 mA. The FGL output power can reach up to 1.8 mW at 399.6 nm corresponding approximately to 3.9 mW at the InGaN LD output facet (see Supplementary Material sec. 3), which is well above reported optical powers for such compact approach in the near-UV spectral range [4–6].

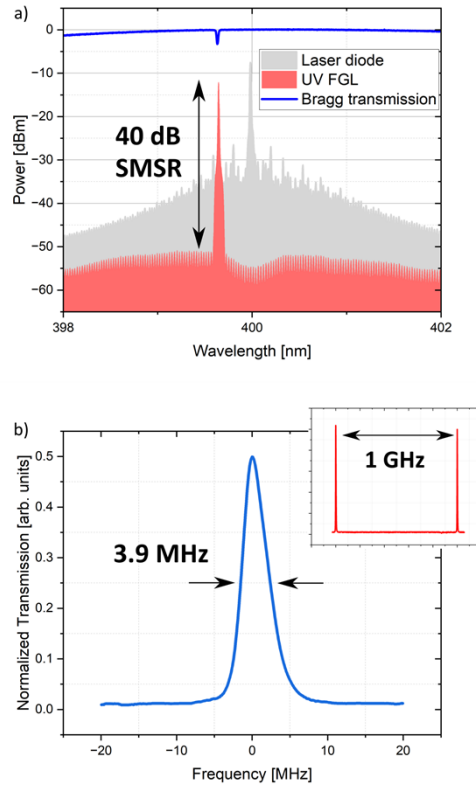


Fig. 4. Spectral characterization of the UV FGL. a) Optical spectra of the laser diode (gray curve) and the UV FGL (red curve) for a pump current of 124 mA. The blue curve corresponds to the fiber Bragg transmission centered at 399.6 nm. b) Optical spectrum of the UV FGL obtained with a FPE (3.9 MHz resolution and 1 GHz FSR). Inset) Optical spectrum measurement through the FPE confirming that the FGL behaves in the single-mode regime.

Since the OSA resolution is not sufficient to prove single-mode operation, the spectral performances of the FGL are then studied using the characterization benches displayed in Fig. 3a). The high-resolution measurements of the optical spectrum were carried out with an FPE. The result is presented in the inset of Fig. 4b). Two peaks separated by 1 GHz, corresponding to the FSR of the FPE, confirmed that the FGL oscillates on a single mode of the external cavity. However, as the width of the measured peak (3.9 MHz) corresponds to the resolution of the FPE, this feature cannot be used to evaluate correctly the linewidth.

3.2 Low frequency noise behavior

A self-homodyne [17] characterization bench based on a Mach-Zehnder [30] interferometer was built (Fig. 3a)) to determine the actual frequency noise (FN) of the laser. This setup enables laser FN analysis over a frequency bandwidth ranging from 100 Hz to 2 MHz. The noise floor is rated at around 40 Hz²/Hz. Fig. 5a) shows the result of the measurements. The red curve represents the characterization of the FN of the UV FGL laser at 399.6 nm. For the sake of comparison, the FN of a commercial external cavity diode laser (ECDL, model Toptica DL Pro) used for Sr-ion cooling and Rb Rydberg excitation at 420.0 nm is shown (blue curve). Usually, the frequency noise of a laser is characterized by a white noise of amplitude h_0 at high frequencies, which refers to the intrinsic linewidth of the laser, and the noise at low frequencies (f), whose slope changes in $\frac{1}{f^\alpha}$ with $1 < \alpha < 2$ corresponds to slow frequency drifts of the

intrinsic linewidth [31]. This last contribution is associated with the Gaussian profile which, convolved with the Lorentzian shape intrinsic linewidth, gives the Voigt profile of the laser [32]. It is possible, from measurements of the FN, to estimate the laser linewidth using the Elliott formula [33] (see Supplementary Material Sec. 4).

The FN of the FGL exhibits a plateau for frequency values above 300 kHz corresponding to the white noise associated with the intrinsic linewidth of the laser, which is mainly determined by the noise due to spontaneous emission. A value of $h_0 = 4149 \text{ Hz}^2/\text{Hz}$ gives an estimate of the intrinsic linewidth, through the Elliott formula, on the order of $14 \pm 2 \text{ kHz}$. The corresponding reconstructed Lorentzian-shape intrinsic linewidth is shown in Fig. 5b) (red curve). The intrinsic linewidth is about one order of magnitude smaller than that of the Toptica DL Pro linewidth ($120 \pm 19 \text{ kHz}$). In comparison to recently reported works dealing with compact external cavity semiconductor laser structures [4–6] within the wavelength range of 380-420 nm, our measurements exhibit a significant improvement of at least two orders of magnitude.

The integration of the FN spectral density and in particular the low-frequency contribution gives access to an estimate of the Voigt profile with a linewidth on the order of $720 \pm 120 \text{ kHz}$ similar to the performances of the Toptica DL Pro. Indeed, acoustic and mechanical noises perturb the FGL central frequency, contributing to the enlargement of the linewidth for longer integration times. Locking the laser to a more stable frequency reference [30] could provide a solution to overcome this technical noise affecting the emission frequency.

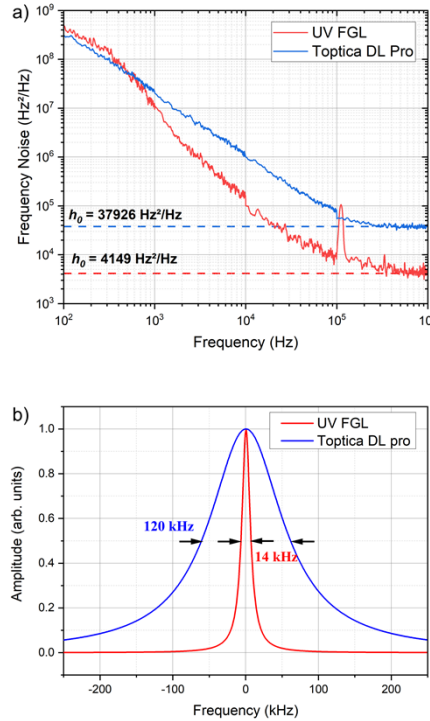


Fig. 5. a) Frequency noise measurements of the UV FGL at 399.6 nm (red color) and Toptica DL Pro emitting at 420.0 nm (blue color). The peak seen at $\sim 100 \text{ kHz}$ on the red curve is due to the photodiode noise. b) Reconstructed optical spectrum from frequency noise measurements by making use of the Elliott formula. Details are given in the Supplementary Material (sec. 4).

4. Conclusions

By butt-coupling an InGaN semiconductor laser diode emitting near 400 nm to an FBG, a compact narrow-linewidth semiconductor laser with a Lorentzian linewidth as low as 14 kHz corresponding to a white frequency noise below 5000 Hz²/Hz is demonstrated. This mW-output power laser fulfills the low-frequency noise performances required for atomic spectroscopy and frequency metrology, offering the possibility to develop compact optical atomic clocks [11] and portable quantum sensors [34] based on electronic transitions occurring in the near-UV range [15] as for example, the excitation of the ytterbium Rydberg state at 399 nm for quantum information processing. The compactness, wavelength versatility and ease of access of the fibered output signal should favor the hybridization of such an FGL to integrated photonic platforms for quantum information processing [35,36].

Funding. UV4Life (19005486), the European Regional Development Fund (EU000998), ANR COMBO (ANR-18-CE24-0003), and Labex Cluster of Excellence FIRST-TF (ANR-10-LABX-48-01) for the LEILA project.

Acknowledgments. The authors acknowledge the useful discussions with Monique Thual, Jean-Claude Simon, and Edgar Casta. The authors would like to thank Mathilde Gay, Laurent Bramerie, and Sebastien Lobo for their technical support in the laboratory.

Disclosures. The authors declare no conflicts of interest.

Data availability. Data underlying the results presented in this paper are not publicly available at this time but may be obtained from the authors upon reasonable request.

Supplemental document. See [Supplement 1](#) for supporting content.

References

1. C. Porter, S. Zeng, X. Zhao, and L. Zhu, "Hybrid integrated chip-scale laser systems," *APL Photonics* **8**, 080902 (2023).
2. W. Liang, V. S. Ilchenko, D. Eliyahu, A. A. Savchenkov, A. B. Matsko, D. Seidel, and L. Maleki, "Ultralow noise miniature external cavity semiconductor laser," *Nat. Commun.* **6**, 7371 (2015).
3. W. Loh, F. J. O'Donnell, J. J. Plant, M. A. Brattain, L. J. Missaggia, and P. W. Juodawlkis, "Packaged, High-Power, Narrow-Linewidth Slab-Coupled Optical Waveguide External Cavity Laser (SCOWECL)," *IEEE Photonics Technol. Lett.* **23**, 974–976 (2011).
4. A. Siddharth, T. Wunderer, G. Lihachev, A. S. Voloshin, C. Haller, R. N. Wang, M. Teepe, Z. Yang, J. Liu, J. Riemensberger, N. Grandjean, N. Johnson, and T. J. Kippenberg, "Near ultraviolet photonic integrated lasers based on silicon nitride," *APL Photonics* **7**, 046108 (2022).
5. M. Corato-Zanarella, A. Gil-Molina, X. Ji, M. C. Shin, A. Mohanty, and M. Lipson, "Widely tunable and narrow-linewidth chip-scale lasers from near-ultraviolet to near-infrared wavelengths," *Nat. Photonics* **17**, 157–164 (2023).
6. C. A. A. Franken, W. A. P. M. Hendriks, L. V. Winkler, M. Dijkstra, A. R. do Nascimento Jr, A. van Rees, M. R. S. Mardani, R. Dekker, J. van Kerkhof, P. J. M. van der Slot, S. M. García-Blanco, and K.-J. Boller, "Hybrid integrated near UV lasers using the deep-UV Al₂O₃ platform," *arXiv:2302.11492*, <https://doi.org/10.48550/arXiv.2302.1492> (2023).
7. P. S. Donvarkar, A. Savchenkov, and A. Matsko, "Self-injection locked blue laser," *J. Opt.* **20**, 045801 (2018).
8. A. Congar, M. Gay, G. Perin, D. Mammez, J.-C. Simon, P. Besnard, J. Rouvillain, T. Georges, L. Lablonde, T. Robin, and S. Trebaol, "Narrow linewidth near-UV InGaN laser diode based on external cavity fiber Bragg grating," *Opt. Lett.* **46**, 1077–1080 (2021).
9. D. J. Blumenthal, "Photonic integration for UV to IR applications," *APL Photonics* **5**, 020903 (2020).
10. Z. L. Newman, V. Maurice, T. Drake, J. R. Stone, T. C. Briles, D. T. Spencer, C. Fredrick, Q. Li, D. Westly, B. R. Ilic, B. Shen, M.-G. Suh, K. Y. Yang, C. Johnson, D. M. S. Johnson, L. Hollberg, K. J. Vahala, K. Srinivasan, S. A. Diddams, J. Kitching, S. B. Papp, and M. T. Hummon, "Architecture for the photonic integration of an optical atomic clock," *Optica* **6**, 680–685 (2019).

11. V. Maurice, Z. L. Newman, S. Dickerson, M. Rivers, J. Hsiao, P. Greene, M. Mescher, J. Kitching, M. T. Hummon, and C. Johnson, "Miniaturized optical frequency reference for next-generation portable optical clocks," *Opt. Express* **28**, 24708–24720 (2020).
12. A. Gusching, J. Millo, I. Ryger, R. Vicarini, M. A. Hafiz, N. Passilly, and R. Boudot, "Cs microcell optical reference with frequency stability in the low 10^{-13} range at 1 s," *Opt. Lett.* **48**, 1526–1529 (2023).
13. A. A. Savchenkov, J. E. Christensen, D. Hucul, W. C. Campbell, E. R. Hudson, S. Williams, and A. B. Matsko, "Application of a self-injection locked cyan laser for barium ion cooling and spectroscopy," *Sci. Rep.* **10**, 16494 (2020).
14. N. Poli, M. Schioppo, S. Vogt, St. Falke, U. Sterr, Ch. Lisdat, and G. M. Tino, "A transportable strontium optical lattice clock," *Appl. Phys. B* **117**, 1107–1116 (2014).
15. K. Enomoto, N. Hizawa, T. Suzuki, K. Kobayashi, and Y. Moriawaki, "Comparison of resonance frequencies of major atomic lines in 398–423 nm," *Appl. Phys. B* **122**, 126 (2016).
16. Z. L. Newman, V. Maurice, C. Fredrick, T. Fortier, H. Leopardi, L. Hollberg, S. A. Diddams, J. Kitching, and M. T. Hummon, "High-performance, compact optical standard," *Opt. Lett.* **46**, 4702–4705 (2021).
17. R. Kashyap, *Fiber Bragg Gratings*, 2nd edition (Academic Press, New York, 2009).
18. J.-L. Archambault and S. G. Grubb, "Fiber gratings in lasers and amplifiers," *J. Light. Technol.* **15**, 1378–1390 (1997).
19. S. A. Vasil'ev, O. I. Medvedkov, I. G. Korolev, A. S. Bozhkov, A. S. Kurkov, and E. M. Dianov, "Fibre gratings and their applications," *Quantum Electron.* **35**, 1085–1103 (2005).
20. C. R. Giles, "Lightwave applications of fiber Bragg gratings," *J. Light. Technol.* **15**, 1391–1404 (1997).
21. J. I. Hashimoto, T. Takagi, T. Kato, G. Sasaki, M. Shigehara, K. Murashima, M. Shiozaki, and T. Iwashima, "Fiber-Bragg-grating external cavity semiconductor laser (FGL) module for DWDM transmission," *J. Light. Technol.* **21**, 2002–2009 (2003).
22. X. Li, J. Shi, L. Wei, K. Ding, Y. Ma, K. Sun, Z. Li, Y. Qu, L. Li, Z. Qiao, G. Liu, L. Zeng, and D. Xu, "Research Progress of Wide Tunable Bragg Grating External Cavity Semiconductor Lasers," *Materials* **15**, 8256 (2022).
23. C. D. Macrae, K. Bongs, and M. Holynski, "Optical frequency generation using fiber Bragg grating filters for applications in portable quantum sensing," *Opt. Lett.* **46**, 1257–1260 (2021).
24. J. Dorsaz, A. Castiglia, G. Cosendey, E. Feltn, M. Rossetti, M. Duellk, C. Velez, J.-F. Carlin, and N. Grandjean, "AlGaIn-Free Blue III–Nitride Laser Diodes Grown on *c*-Plane GaN Substrates," *Appl. Phys. Express* **3**, 092102 (2010).
25. C. Eichler, S.-S. Schad, F. Scholz, D. Hofstetter, S. Miller, A. Weimar, A. Lell, and V. Harle, "Observation of temperature-independent longitudinal-mode patterns in violet-blue InGaIn-based laser diodes," *IEEE Photonics Technol. Lett.* **17**, 1782–1784 (2005).
26. B. Berrang, L. Polz, R. Kuttler, J. Bartschke, and J. Roths, "FBG inscription in non-hydrogenated SMF28 fiber with a ns Q-switched Nd:VO₄ laser at 213 nm," in *Fifth European Workshop on Optical Fibre Sensors* (SPIE), Vol. **8794**, 309–312 (2013).
27. M. Becker, J. Bergmann, S. Brückner, M. Franke, E. Lindner, M. W. Rothhardt, and H. Bartelt, "Fiber Bragg grating inscription combining DUV sub-picosecond laser pulses and two-beam interferometry," *Opt. Express* **16**, 19169–19178 (2008).
28. K. Zhou, M. Dubov, C. Mou, L. Zhang, V. K. Mezentsev, and I. Bennion, "Line-by-Line Fiber Bragg Grating Made by Femtosecond Laser," *IEEE Photonics Technol. Lett.* **22**, 1190–1192 (2010).
29. M. Becker, T. Elsmann, A. Schwuchow, M. Rothhardt, S. Dochow, and H. Bartelt, "Fiber Bragg Gratings in the Visible Spectral Range With Ultraviolet Femtosecond Laser Inscription," *IEEE Photonics Technol. Lett.* **26**, 1653–1656 (2014).
30. G. Perin, D. Mammez, A. Congar, P. Besnard, K. Manamanni, V. Roncin, F. D. Burck, and S. Trebaol, "Compact fiber-ring resonator for blue external cavity diode laser stabilization," *Opt. Express* **29**, 37200–37210 (2021).
31. F. Riehle, *Frequency Standards: Basics and Applications* (Wiley-VCH, Weinheim, 2004).
32. G. M. Stéphan, T. T. Tam, S. Blin, P. Besnard, and M. Têtu, "Laser line shape and spectral density of frequency noise," *Phys. Rev. A* **71**, 043809 (2005).
33. D. S. Elliott, R. Roy, and S. J. Smith, "Extracavity laser band-shape and bandwidth modification," *Phys. Rev. A* **26**, 12–18 (1982).
34. C. L. Degen, F. Reinhard, and P. Cappellaro, "Quantum sensing," *Rev. Mod. Phys.* **89**, 035002 (2017).
35. R. J. Niffenegger, J. Stuart, C. Sorace-Agaskar, D. Kharas, S. Bramhavar, C. D. Bruzewicz, W. Loh, R. T. Maxson, R. McConnell, D. Reens, G. N. West, J. M. Sage, and J. Chiaverini, "Integrated multi-wavelength control of an ion qubit," *Nature* **586**, 538–542 (2020).
36. K. K. Mehta, C. Zhang, M. Malinowski, T.-L. Nguyen, M. Stadler, and J. P. Home, "Integrated optical multi-ion quantum logic," *Nature* **586**, 533–537 (2020).